Linear Models: Useful Tools to Analyze GCM Results

C. J. KOK AND J. D. OPSTEEGH

Royal Netherlands Meteorological Institute, P.O. Box 201, De Bilt, The Netherlands

H. M. VAN DEN DOOL

University of Maryland, College Park, MD 20742

(Manuscript received 17 March 1986, in final form 17 February 1987)

ABSTRACT

Using a two-level linear, steady state model, we diagnose the 40-day mean response of a GCM to a tropical sea surface temperature (SST) anomaly. The time-mean anomalies produced by the GCM are simulated as linear responses to the anomalous hemispheric distributions of latent heating, sensible heating and transient eddy forcing. Also, the anomalous effect of mountains, caused by anomalies in the zonal mean surface wind is taken into account. All anomalies are defined as the difference between perturbation and control runs. For our analysis, we have taken the tropical Atlantic SST anomaly experiment performed by Rowntree.

We have compared the linear model's response in temperature at 600 mb and winds at 400 mb with the same anomalous quantities produced by the GCM. The similarity between the time-mean anomalies of the GCM experiment and the linear model's response is very high. The pattern correlation coefficients are between 0.6 and 0.7 in the region between 30°N and 60°N. The response to each of the anomalous forcings separately is positively correlated with the GCM anomaly pattern. The amplitude of the response to anomalous forcing by transient eddies is a factor of two to three larger than the effects of anomalous sensible and latent heating. The anomalous effect of the orography is negligible.

Although intended to be a tropical SST anomaly GCM experiment, the difference between control and perturbation runs does not seem to be directly related to tropical heating near the SST anomaly. Instead, most of the forcing of anomalies in the midlatitudes took place in the midlatitudes itself and, in particular, the remote effects of forcing by tropical latent heat sources were minor.

1. Introduction

In a recent paper by Kok and Opsteegh (1985, hereafter referred to as KO), an attempt was made to simulate the observed seasonal mean circulation patterns during 1982 and 1983 as a result of observed tropical diabatic heating, orographic and transient eddy effects. The method they used is called the "response method" by Holopainen (1984); that is, a more or less simplified form of the equations for time-mean flow is used to compute the steady-state response to various prescribed time-mean forcings. If the equations for time-mean flow are sufficiently linear, the effect of each of the forcing mechanisms can be studied in isolation. The method was first used by Youngblut and Sasamori (1980) and by Opsteegh and Vernekar (1982) to study the net effect of transient eddy fluxes on the climatological winter mean stationary waves in the Northern Hemisphere. Both papers indicate that the assumption of linear behavior of stationary planetary waves is realistic at these time scales. This was also shown from observations, at least for the upper part of the troposphere, by Lau (1979).

In KO, the response method was applied to relate observed *anomalies* in the circulation to the *anomalies* in various forcing mechanisms. The results were systematically verified. It was found that the response to forcing by transient eddies is large for all seasons considered and that it correlates significantly with observed anomalies.

In this paper, a similar experiment is performed. Instead of simulating observed atmospheric anomalies, we will attempt to simulate the difference between a control and a perturbation run with a general circulation model (GCM). We use the tropical Atlantic sea-surface temperature (SST) anomaly experiment performed by Rowntree (1976, hereafter referred to as R). The control run was an 80-day integration with normal January SSTs using real initial data. In the perturbation run the SST anomaly in the tropical Atlantic as observed in January 1963 was added to the normal SST field. Anomaly fields are obtained by subtracting the day 40 to 80 mean fields of the control run from the same fields of the perturbation run. Rowntree's experiment is quite interesting in that it seems to attribute the observed positive anomalous sea level pressure over the midlatitude Atlantic in January 1963 (leading to record low temperatures in Europe) to SST anomalies in the tropical Atlantic.

The model we use to analyse Rowntree's results is

a linear two-layer steady-state model. We will compute the model's response to forcing by anomalies in the transient eddy fluxes, latent heating and sensible heating, these fields being known from the GCM experiment. The forcing due to anomalous radiation will, unfortunately, not be considered here as it was not stored on history tapes while running the GCM. Also the anomalous effect of mountains, caused by anomalies in the zonal mean surface wind, will be taken into account. The response of the linear model to any combination of these four forcing mechanisms will be referred to as model anomalies, as opposed to the "observed" anomalies derived from Rowntree's experiment. In this paper, we will compare modeled and observed temperature anomalies at 600 mb and wind anomalies at 400 mb.

The advantage of dealing with a GCM instead of real atmospheric anomalies is, obviously, that the anomalous forcing components can be calculated accurately, whereas atmospheric forcing is difficult to assess from real data over large parts of the globe. This makes it much easier to study relations between surface conditions and anomalies in time-mean circulation patterns as well as the relative importance of the various forcing mechanisms in creating these anomalies. In this particular case, we hope to answer the question of how important the Atlantic SST anomalies have been in creating a seemingly realistic difference between two GCM runs. It is hoped that the GCM resembles the real atmosphere sufficiently well so that the results have some general validity.

In summary, the goal of this paper is twofold. On the one hand, we want to use data from GCM runs to test the validity of the assumptions underlying linear models. And secondly, we want to show that using a linear model to postprocess the GCM output is very useful in understanding what has been going on in the GCM.

2. The linear model

The model used in this study is described by Opsteegh and Van den Dool (1980) and more recently in KO. It is based on the equations for time-mean flow linearized around a zonal mean basic state. We neglect tendency terms, the terms that describe the interaction of the anomalies with the stationary eddies and the nonlinear terms in the time-mean anomalies. The equations are

Zonal momentum balance:

$$\frac{U_{sn}}{a\cos\phi}\frac{\partial\hat{u}}{\partial\lambda}+\frac{\partial U_{sn}}{a\partial\phi}\hat{v}+\frac{\partial U_{sn}}{\partial p}\hat{\omega}-f\hat{v}+\frac{1}{a\cos\phi}\frac{\partial\hat{\Phi}}{\partial\lambda}-\hat{F}_{Wx}=\hat{F}_{Ex} \quad (1)$$

Meridional momentum balance:

$$\frac{U_{sn}}{a\cos\phi}\frac{\partial\hat{v}}{\partial\lambda}+f\hat{u}+\frac{1}{a}\frac{\partial\hat{\Phi}}{\partial\phi}-\hat{F}_{Wy}=\hat{F}_{Ey} \quad (2)$$

First law of thermodynamics:

$$\frac{U_{sn}}{a\cos\phi}\frac{\partial\hat{T}}{\partial\lambda}+\frac{\partial T_{sn}}{a\partial\phi}\hat{v}-\sigma_{sn}\hat{\omega}+\delta\hat{T}=\frac{\hat{Q}}{c_P}+\hat{Q}_E \quad (3)$$

Continuity equation:

$$\frac{1}{a\cos\phi}\frac{\partial\hat{u}}{\partial\lambda}+\frac{1}{a\cos\phi}\frac{\partial}{\partial\phi}(\hat{v}\cos\phi)+\frac{\partial\hat{\omega}}{\partial p}=0 \quad (4)$$

Hydrostatic approximation:

$$\frac{\partial\hat{\Phi}}{\partial p}=-\hat{\alpha} \quad (5)$$

Equation of state:

$$p\hat{\alpha}=R\hat{T}. \quad (6)$$

Here U_{sn}, T_{sn} and σ_{sn} are the zonal mean wind, temperature and static stability, respectively. The model variables for the anomalies are $\hat{u}$, $\hat{v}$, $\hat{\omega}$, $\hat{\Phi}$, $\hat{T}$, $\hat{\alpha}$; these symbols have their usual meaning. The $\hat{F}_{Wx}$, $\hat{F}_{Wy}$ are linear dissipation terms, with coefficients of 2×10^{-6} at 800 mb and 10^{-7} at 400 mb. Following Simmons (1982), the value of these coefficients is increased in the vicinity of zero wind lines to

$$\frac{\cos^2\phi}{2U_{sn}^2}\times10^{-5}\ \mathrm{s}^{-1}$$

wherever they fall below this value. The Newtonian cooling coefficient δ is entirely described by this formula for the singular line dissipation. Since our zonal mean basic state does not have a zero wind line (as is shown in section 3), the inclusion of singular line dissipation is of minor importance to our results. The $\hat{F}_{Ex}$, $\hat{F}_{Ey}$ and $\hat{Q}_E$ are anomalous asymmetrical transient eddy forcing terms of momentum and heat, and $\hat{Q}$ is the anomalous diabatic heating.

The momentum and continuity equations are applied at 800 and 400 mb and the thermodynamic equation at 600 mb. The model has a rigid boundary at 200 mb ($\hat{\omega}=0$). The lower boundary condition is applied at 1000 mb where the vertical velocity (ω_0) is that produced by the zonally-averaged zonal surface airflow over the mountains. In experiments without mountains, ω_0 is taken to be zero. At the equator, we apply symmetry conditions.

The model is semispectral: the variables are expressed in Fourier components along latitude circles, while a gridpoint representation is used in the meridional direction.

For further details about the model, we refer the reader to Opsteegh and Van den Dool (1980) and KO.

3. Data and experimental design

Rowntree performed a tropical Atlantic ocean temperature anomaly experiment with a 5-layer hemi-

spheric GCM. The experiment considered here consisted of a control run (called C3 in Rowntree's paper) in which normal January sea surface temperatures (SSTs) were used, and a perturbation run (A3) in which the tropical Atlantic SST anomaly of January 1963 was added to the climatological SST field. This anomaly covered virtually the entire Atlantic south of 30°N and had a maximum of more than 2 K at 18°N close to the African coast. The SST anomaly was the only difference between the two runs. In both runs, the model was integrated for 80 days using initial data for 29 December 1965. For details about the GCM, the reader is referred to R and references thereof.

The anomalies to be modeled were obtained by subtracting the time mean response of day 41 to 80 of the control run from that of the perturbation run. Similarly the anomalies in the 40-day mean forcing components were computed as the difference of the time-mean forcing in perturbation and control runs. We deal with the effects of internal forcing by transient eddies, sensible and latent heating and of mountains. The only missing forcing mechanism is the radiation (not available). We first drive the linear steady-state model with all these forcings combined. Next, the effect of each of the forcings is studied separately. In this study, only the first six zonal wavenumbers (m = 1 to 6) of the forcing fields are retained.

As a basic state for the linear model (U_{sn}, T_{sn} and σ_{sn}), we use the zonal mean fields of the perturbation run. Additional experiments using the basic state of the control run gave approximately the same results. The 40-day mean zonally averaged zonal winds at 400 and 800 mb of the perturbation run are displayed in Fig. 1. Comparison with the observed climatological mean January winds at these heights (not shown) shows that the model's jet is too strong and is shifted to the north by about 10 degrees. As can be seen from the small difference (dash-dotted line), the control and perturbation runs have this rather large systematic error in common. Another shortcoming of the perturbation run (and of the control run as well) is the absence of tropical easterlies. The absence of easterlies in the tropics and the use of symmetry conditions at the equator cause the equator to act as a reflecting wall.

The transient eddy effects on the mean flow can be expressed as forces in the momentum equations and heating in the thermodynamic equation. The forcing can be written as follows:

$$F_{Ex} = -\left(\frac{1}{a\cos\phi}\frac{\partial\overline{u'^2}}{\partial\lambda} + \frac{1}{a}\frac{\partial\overline{u'v'}}{\partial\phi} + \frac{\partial\overline{u'\omega'}}{\partial p} - \frac{2\tan\phi}{a}\overline{u'v'}\right), \tag{7}$$

$$F_{Ey} = -\left(\frac{1}{a\cos\phi}\frac{\partial\overline{u'v'}}{\partial\lambda} + \frac{1}{a}\frac{\partial\overline{v'^2}}{\partial\phi} + \frac{\partial\overline{v'\omega'}}{\partial p} + \frac{\tan\phi}{a}(\overline{u'^2} - \overline{v'^2})\right), \tag{8}$$

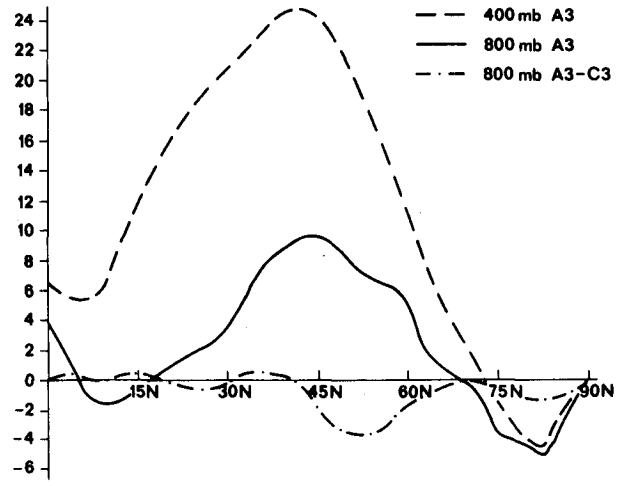

FIG. 1. 40-day mean zonally averaged zonal winds at 400 and 800 mb of the GCM perturbation run. The dashed–dotted line displays the difference at 800 mb between control and perturbation run.

$$Q_E = -\left(\frac{1}{a\cos\phi}\frac{\partial\overline{u'T'}}{\partial\lambda} + \frac{1}{a}\frac{\partial\overline{v'T'}}{\partial\phi} + \frac{\partial\overline{\omega'T'}}{\partial p} - \frac{R}{pc_p}\overline{\omega'T'} - \overline{v'T'}\frac{\tan\phi}{a}\right), \tag{9}$$

where the overbar is a 40-day mean operator and the primes are deviations from the 40-day means. Expressions (7) and (8) are applied at 400 and 800 mb; (9) at 600 mb.

The fields were smoothed in the meridional direction by applying three times a three-point smoothing operator. We have ignored the vertical flux convergence terms. North of 70°N, we have neglected anomalous forcing since linearity breaks down for small values of the basic state zonal winds. Consequently, a forcing at those latitudes gives rise to very large and unrealistic responses. Between 60 and 70 degrees, the forcing fields are tapered by a factor which decreases linearly from one to zero.

Figure 2 displays the spectrally truncated (m = 1 to 6) anomalous transient eddy forcing fields. In all fields, the highest values of the anomalies occur in the midlatitudes. The forcing is particularly large over the Pacific and United States. It is evident from Fig. 2 that $\hat{F}_{Ex}$ and $\hat{F}_{Ey}$ have more or less the same pattern at 400 and 800 mb.

In Fig. 3a, we show the zonally-asymmetric part (m = 1 to 6) of the 40-day mean anomalous sensible heat flux at the earth's surface, while in Fig. 3b the anomalous precipitation is displayed. The sensible heat flux shows extremes over the oceans near the midlatitudinal coasts where normal air–sea temperature contrasts are large. Ironically the anomalous sensible heating in the area of the SST anomaly is very small. The distribution of the anomalous precipitation is not obviously related to the SST anomaly either. As is the case with the

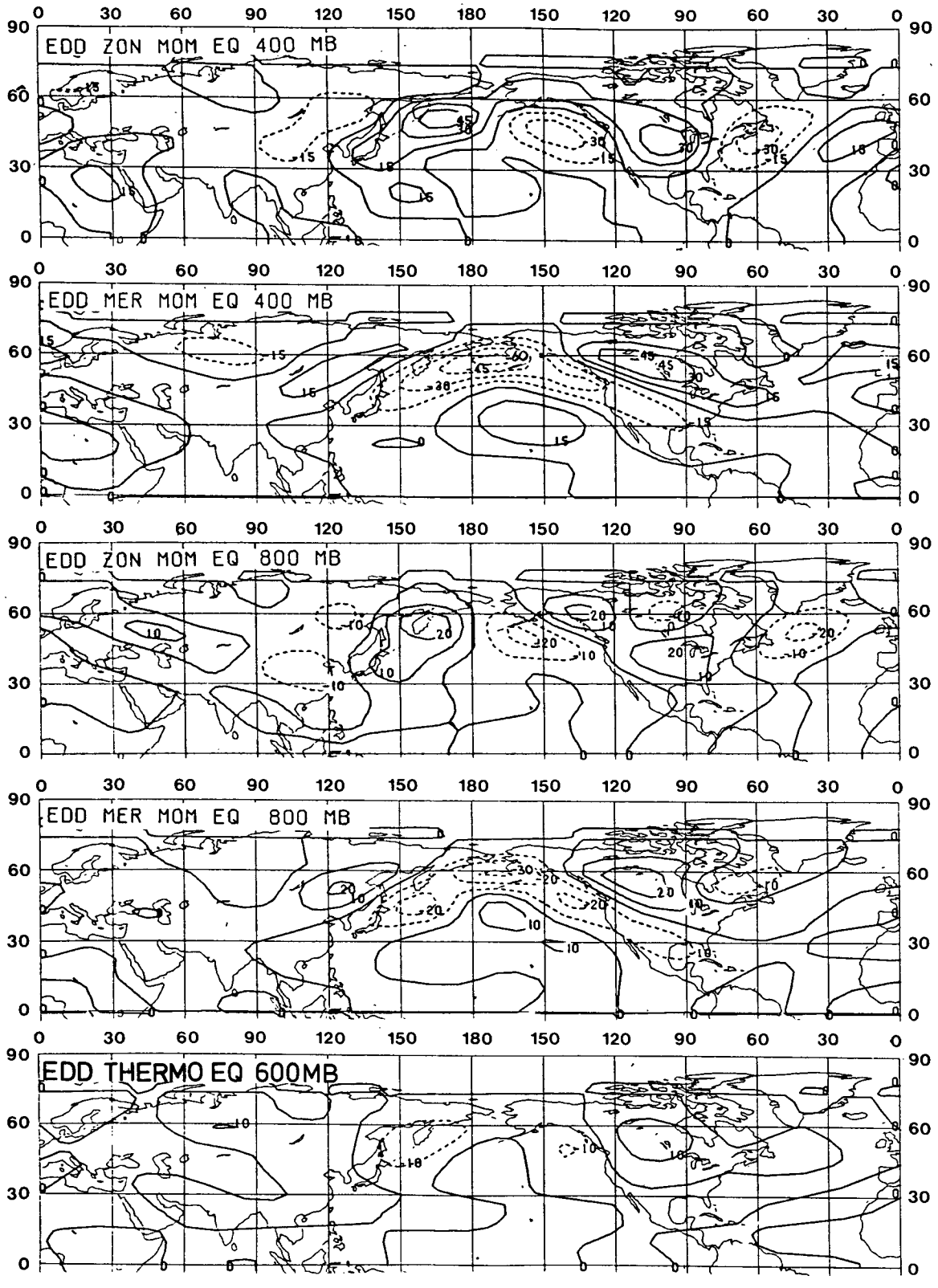

FIG. 2. Hemispheric distribution of the internal forcing by transient eddies. The upper two figures show the forcing in the zonal and meridional momentum equations at 400 mb respectively. The next two figures show the same forcing fields at 800 mb. The bottom figure shows the forcing in the thermodynamic equation at 600 mb. Only zonal wavenumber 1 to 6 have been retained. Units are 10^{-6} m s^{-2} for the upper four figures and 10^{-6} K s^{-1} for the bottom figure.

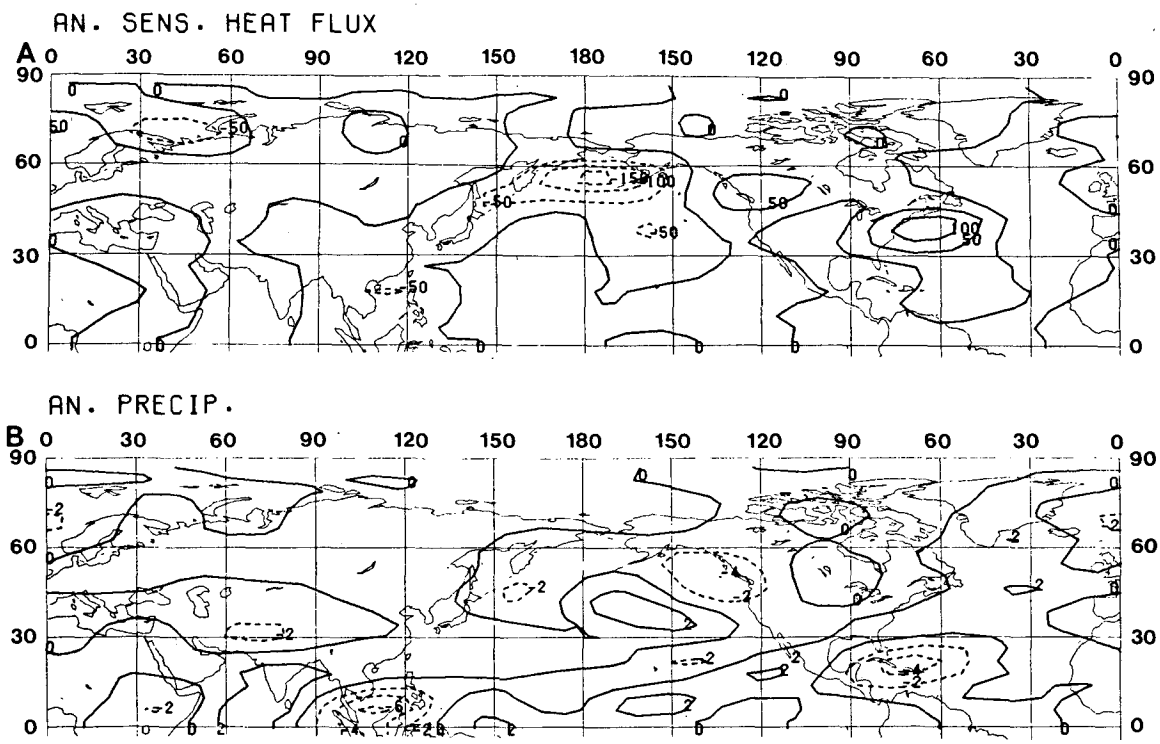

FIG. 3. The zonally asymmetrical part (m = 1 to 6) of the anomalous sensible heat flux at the surface (a) and anomalous rainfall (b) produced by the GCM as a response to a tropical SST anomaly. Units are J m^{-2} s^{-1} and mm day^{-1} respectively. Values of 100 J m^{-2} s^{-1} and 4 mm day^{-1} correspond to a heating of 10^{-5} K s^{-1} in the linear model's temperature equation.

anomalous sensible heat flux, the largest differences with the control run occur over the oceans, but now anomalies in the tropics dominate. There is a particularly strong negative anomaly over Indonesia.

The most striking aspect of Fig. 3 is that a simple relation between the SST anomaly in the Atlantic and the time-mean sensible and latent heating anomalies does not seem to exist at all.

The anomalies in time-mean sensible and latent heating were not directly available and had to be estimated from the anomalies in sensible heat flux at the surface and precipitation. In our two-layer model, we need the vertical mean value of the anomalous diabatic heating $\hat{Q}$. The sensible heating is computed with

$$\hat{Q}_{SH}/c_p = \frac{g}{c_p}\frac{1}{p_0}\int_{p=0}^{p=p_0}\frac{\partial \hat{H}}{\partial p}\,dp = \frac{g}{c_p}\frac{\hat{H}_0}{p_0},$$

where $\hat{H}$ is the anomalous heat flux, p_0 is surface pressure and H_0 the surface heat flux. This gives a vertical mean heating $\hat{Q}/c_p$ of 10^{-5} K s^{-1} or about 1 K day^{-1} when H_0 = 100 J m^{-2} s^{-1}. For latent heating, we assume that 4 mm of precipitation per day results in a vertical mean heating of 10^{-5} K s^{-1}. The same procedure as in the case of transient eddy forcing was used to suppress the heat forcings at high latitudes.

The anomalous effect of mountains is incorporated in the model by means of a vertical velocity at the lower boundary due to the surface zonal airflow over the mountains. The zonal mean wind at the surface was taken to be half the 40-day mean wind speed at 800 mb of the perturbation run, minus that of the control run. We used

$$\hat{\omega}_{1000} = \frac{-\rho_{1000}}{a\cos\phi}\,\frac{U_{A3}-U_{C3}}{2}\,\frac{\partial}{\partial\lambda}gH \qquad (10)$$

where ρ_{1000} is density at 1000 mb, g is gravity, H is topographic height and U is zonal mean 800 mb wind. The anomalous zonal wind at 800 mb is shown by the dashed-dotted line in Fig. 1.

The forcing associated with the Greenland topography has not been taken into account.

4. Results

In this section, the linear responses to the various forcing fields described in the previous section will be presented. After having established the validity of the linear approach on the basis of a simulation experiment using all forcings combined, the significance of the individual forcing fields for the anomalies occurring in Rowntree's GCM experiment will be investigated. The main emphasis will be on the simulation of the anomalous temperature ($\hat{T}$) field at 600 mb, although some model results of anomalous winds at 400 mb will be presented as well. Since zonal wind patterns exhibit large-scale structures in the zonal direction, whereas

meridional wind fields are more determined by higher zonal wavenumbers, we discuss results for both fields separately. The reason for not showing results at 800 mb is that the structure of diabatically forced stationary waves at low levels is very sensitive to the exact vertical profile of the heating, whereas the response at high levels is more determined by the vertically integrated heating (e.g., see Hoskins and Karoly, 1981). In the two-level model, we cannot specify a vertical structure to the heating; hence we deal with the vertically integrated part only.

The degree of similarity between simulated anomalies (A) and the "observed" anomalies (B) occurring in the GCM is measured by means of the pattern correlation coefficient (pcc):

$$\rho(A,B)=\frac{\sum(A\,B)-(\sum A\,\sum B)/N}{\{[\sum A^2-(\sum A)^2/N][\sum B^2-(\sum B)^2/N]\}^{1/2}}; \tag{11}$$

A and B both consist of the first six zonal wavenumbers. The summations are area-weighted by a factor $\cos\phi$. In grid-space $\sum A\,B$ reads as follows:

$$\sum(A\,B)=\sum_{i=1}^{N}\sum_{j=1}^{M}\cos\phi_i A(i,j)B(i,j). \tag{12}$$

Here M and N represent the number of grid points in the zonal and meridional directions. Since we consider the first six waves only and not wavenumber zero, the mean values of A and B are zero.

a. Response to all forcings combined

Figure 4a displays the GCM result for the asymmetrical part of the anomalous 40-day mean temperature at 600 mb. The response is almost entirely determined by two large strong anomalies: a cold anomaly covering all of North America and a warm one centered near 60°N, 150°E. Over western Europe and the eastern Atlantic, the temperature anomalies are quite small. This is a bit surprising in view of the large GCM anomalies in surface pressure (e.g., see Fig. 10 in R). The anomalous geopotential heights at 500 mb as displayed in his Fig. 8 are weak also. Apparently, the anomalies in this area are restricted to a relatively shallow surface layer.

The response of the linear model to all four forcings combined (transient eddy forcing, mountain forcing, sensible and latent heating) is shown in Fig. 4b. The resemblance with the GCM response is striking. The two anomalies between 120°E and 90°W that dominate the response of the GCM are reproduced with approximately the right amplitude, but with a phase error of about 20 degrees to the west. North of 70°N the agreement is less, which is probably due to model deficiencies and the neglect of all forcings at high latitudes. For the region between 30 and 60 degrees, where

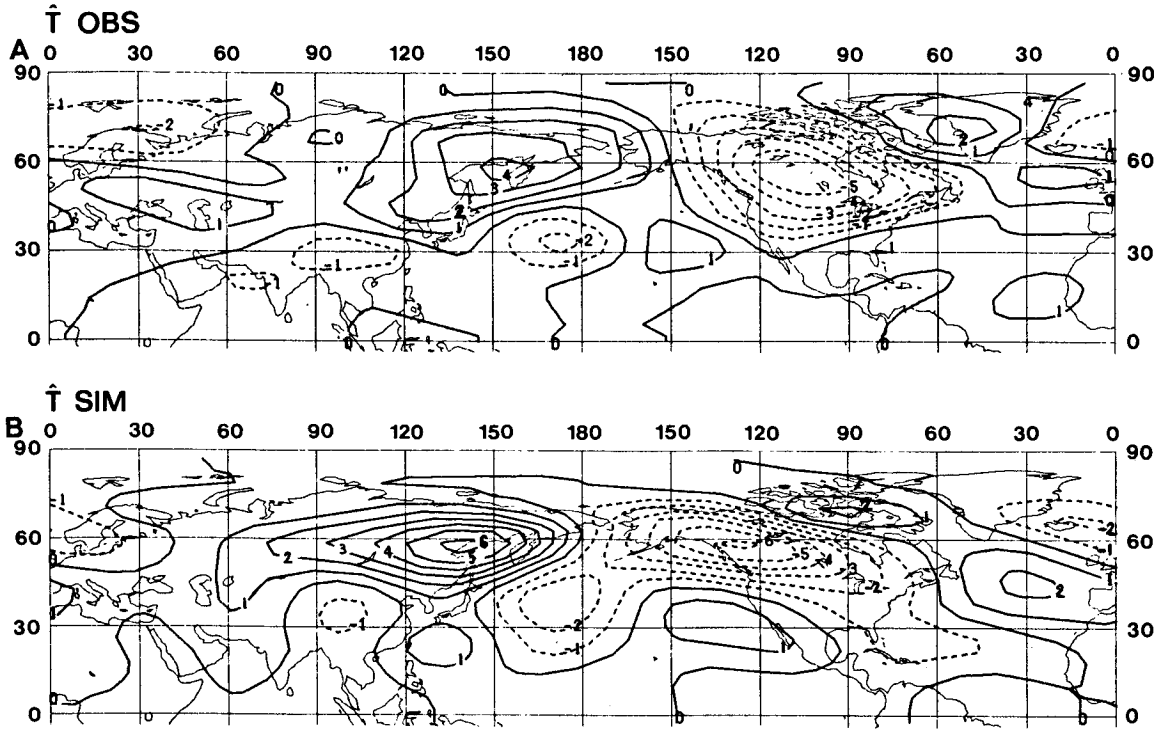

FIG. 4. Anomalous temperature ($\hat{T}$) at 600 mb (m = 1 to 6) produced by the GCM (a) and the linear model (b) as a response to forcing by anomalous sensible heating, latent heating, transient eddy and orographic forcing. Units are in °K.

TABLE 1. Pattern correlation coefficients (pcc) and rms ratios of $\hat{T}$, $\hat{u}$ and $\hat{v}$ for the experiment with all forcings combined. The left part of the table gives the results for the zone between 30° and 60° and the right part for the zone between 0° and 30°N.

	30°–60°N			0°–30°N		
	$\hat{T}$	$\hat{u}$	$\hat{v}$	$\hat{T}$	$\hat{u}$	$\hat{v}$
pcc	0.68	0.63	0.61	0.17	0.51	0.34
rms ratio	1.10	0.75	0.84	1.00	1.25	1.19

the amplitude of the anomalies is large, the pcc is 0.68. In the tropics (0–30°N), where the anomalies in temperature are small, the pcc is 0.17. These values can be found in Table 1, which contains the pcc between the linear model's response to the combined forcings and Rowntree's 40-day mean anomalous temperature and wind fields. The ratios of the root mean square (rms) of the simulated and "observed" fields are also given.

In Fig. 5, we show the observed $\hat{u}$ field together with the simulated $\hat{u}$ for the experiment when all forcings are combined. In contrast to the temperature field, tropical wind anomalies are large in both observed and simulated fields. The similarity between simulated and observed $\hat{u}$ fields is good in both midlatitudes and tropics. The pcc between 30° and 60°N is 0.63, whereas in the tropics the pcc is 0.51 which is much larger than for the low amplitude $\hat{T}$ response (see Table 1). The amplitude in the midlatitudes is underestimated. The strength of the zonal winds at the equator is much too strong. The reason for this discrepancy is unclear, although the weakness of the $\hat{u}$ field in the tropics produced by the GCM suggests that the tropically trapped modes are suppressed in the hemispheric GCM experiment.

Figure 6 displays both the observed and simulated anomalous meridional wind field. Comparison with Fig. 5 shows that the $\hat{v}$ field exhibits a much smaller zonal scale than the anomalous zonal wind pattern. The strength of the $\hat{u}$ and $\hat{v}$ fields is about the same in middle latitudes, but near the equator the zonal winds dominate. The similarity between simulated and observed fields is again fairly good, pcc for the midlatitudes and tropics being 0.61 and 0.34, respectively.

In KO the statistical significance of pcc between observed and simulated seasonal mean $\hat{u}$ and $\hat{v}$ fields was computed for a midlatitudinal strip (30°–60°). The probability distribution of the pcc for experiments with random forcing was established. It is displayed in Fig. 11 of KO, which indicates that pcc of 0.6 or larger have a chance of about one percent to occur. So the results of our simulation between 30° and 60°N, as summarized in Table 1, can be regarded as highly significant. For details about the derivation of the probability distribution we refer to KO.

On the basis of the large similarity between observed

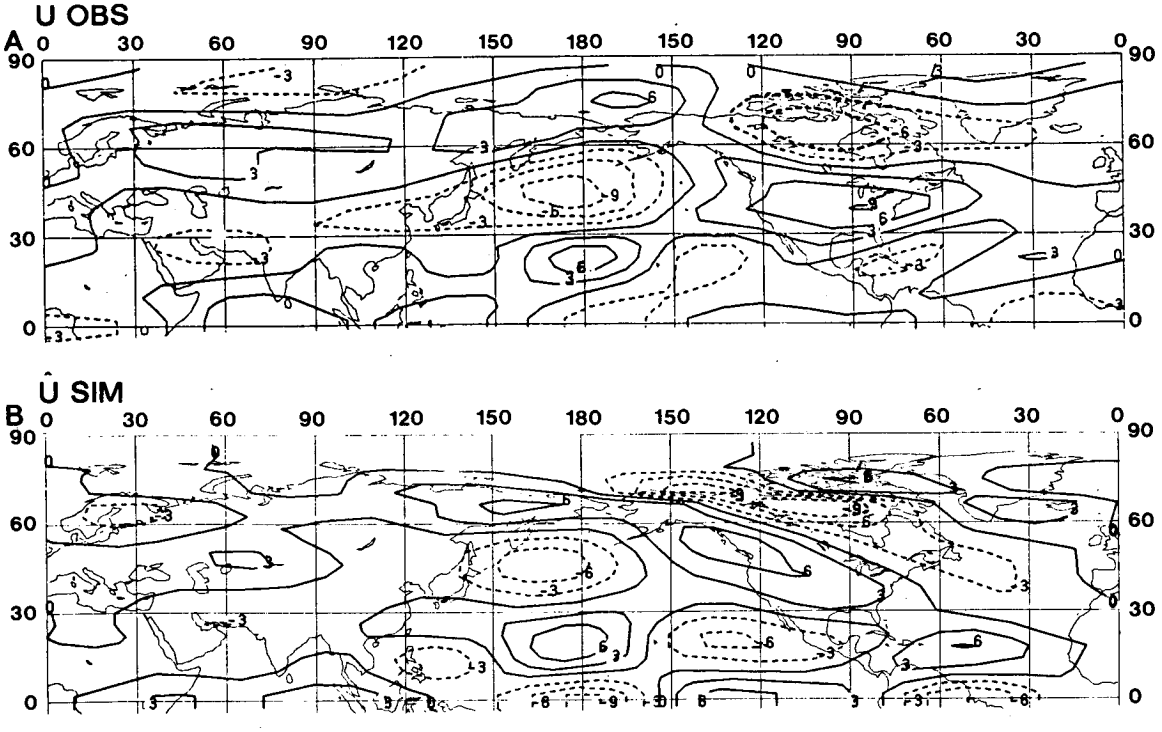

FIG. 5. As in Fig. 4 but for $\hat{u}$ at 400 mb. Units are m s^{-1}.

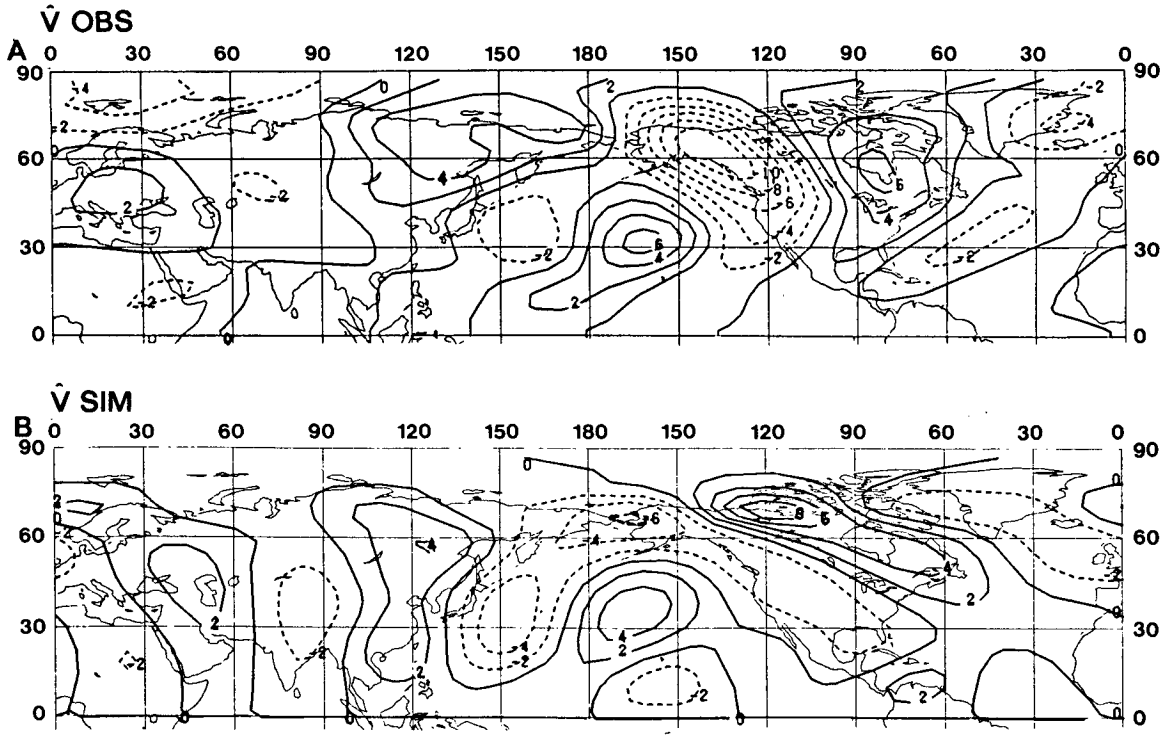

FIG. 6. As in Fig. 4 but for $\hat{v}$ at 400 mb. Units are m s^{-1}.

and simulated $\hat{T}$, $\hat{u}$ and $\hat{v}$ fields, we conclude that anomalies in time-mean circulation patterns can, to first order, be described as a linear response to time-mean anomalous forcings, especially in the midlatitudes. Therefore, it can be justified to look at the responses to individual forcing components. The rms of these responses is a measure of the relative importance of the individual forcings. The total response having a large pcc does not necessarily mean that the response to each of the separate forcings also resembles the observed flow characteristics. Nevertheless, we will not only compare them in terms of rms but also in terms of the pcc.

b. *Effects of separate forcings*

The separate contributions of anomalous forcing by transient eddies, sensible and latent heating to the $\hat{T}$ field at 600 mb are shown in Figs. 7a, b and c respectively. The response to anomalous mountain forcing is not shown because of its small amplitude. The pcc and rms ratios for the experiments with the separate forcings, as well as for all forcings combined, are given in Table 2. The response to anomalous transient eddy forcing is by far the most important in middle and high latitudes. Apparently the transient eddies are the main contributors to the two large anomalies so conspicuously present in Fig. 4a. Both simulated anomalies have westerly phase errors though. The pcc of the total response to transient eddy forcing between 30°N and 60°N is 0.50. The response in the tropics is small as is the pcc (0.11).

In both the experiments with sensible and latent heat forcing only, the two large midlatitudinal anomalies in the $\hat{T}$ response are present approximately in the right position (Fig. 7b, c). Both patterns are therefore positively correlated with the GCM anomalies between 30° and 60°N: pcc being 0.47 and 0.60, respectively. Apparently, all three forcings discussed so far contribute in the same sense to the anomalous temperature pattern. Moreover, each of the forcings is needed to increase the similarity with the anomalous GCM response, especially in terms of magnitude. For instance, the positive anomaly near 60°N, 150°E in the $\hat{T}$ response to transient eddies is doubled in amplitude when the response to diabatic heat forcing is added, while the negative anomaly over North America is broadened.

Also for $\hat{u}$ the similarity improves when the three forcings are combined (Table 2). This is not true for $\hat{v}$, where the relative impact of the diabatic heat sources and sinks on the pcc is small.

In the tropics, the total response to the diabatic heatings is of the same order of magnitude as the separate responses, indicating that, in contrast to the midlatitudes, the two heatings counteract each other to some extent. The orographic effect on the anomalies is small in amplitude both in the tropics and in the extratropics.

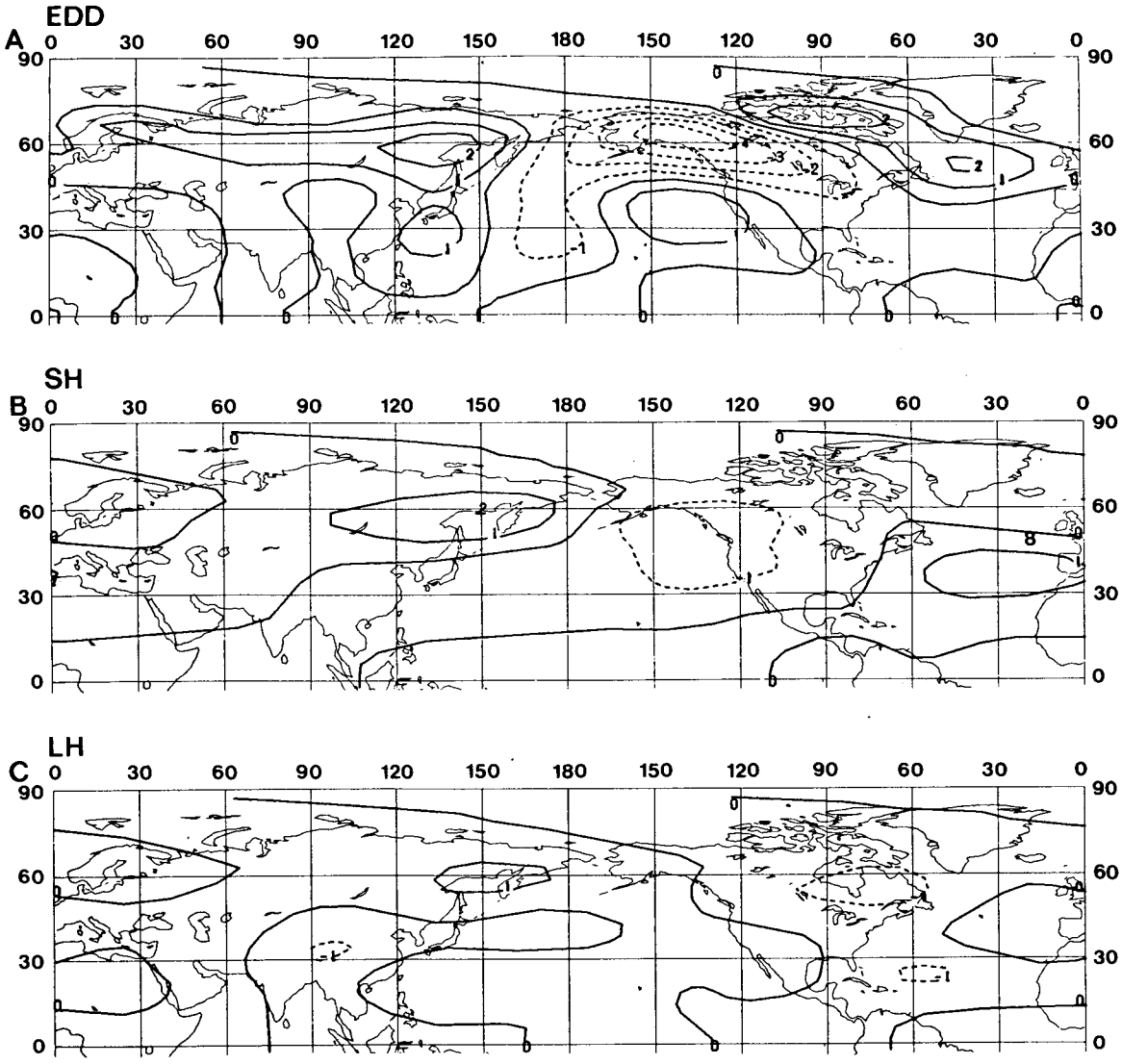

FIG. 7. Response of the linear model in $\hat{T}$ at 600 mb to transient eddy forcing (a), sensible heating (b) and latent heating (c). Units are in °K.

Figure 8 displays for each of the zonal wavenumbers separately the rms and pcc of the various simulation experiments. We focus here on the area 30° to 60°N. The figure shows the results for $\hat{T}$ at 600 mb and $\hat{u}$ and $\hat{v}$ at 400 mb for experiments where the model is driven by all forcings (left column), by transient eddy forcing only (middle column) and by sensible and latent heating combined (right column). Dashed lines show the rms as a function of zonal wavenumber for the linear model's results, solid lines show the same quantity for the GCM experiment. The pcc are given by crosses.

It is clear that when all forcings are combined, the amplitudes of the various zonal wavenumbers of $\hat{T}$ are in good agreement with the observed amplitudes. The response in all zonal wavenumbers is positively correlated with the corresponding wavenumbers in the observed field. For $\hat{u}$ and $\hat{v}$ the first five zonal wavenumbers correlate very well. The rms value for each wavenumber of the simulated anomalous winds is again close to the observed rms except for $m = 1$.

The relative contribution of the diabatic heatings to the total response in $\hat{T}$, $\hat{u}$ and $\hat{v}$ is substantial for the largest two zonal waves only, whereas the impact of the transient eddies is significant for all zonal waves. Especially for wavenumber 3 and larger this forcing appears to be more important than all other forcings. Figure 8 shows that exactly for the scales for which transient eddies or diabatic heat sources are important, the pcc for the appropriate wavenumbers are high; only the first three zonal wavenumbers of the response to sensible and latent heating correlate well with observations, while the pcc for the response to transient eddy

TABLE 2. As in Table 1 but for experiments with all forcings combined and separately.

	30°–60°N			0°–30°N		
Forcing	$\hat{T}$	$\hat{u}$	$\hat{v}$	$\hat{T}$	$\hat{u}$	$\hat{v}$
			pcc			
Total	0.68	0.63	0.61	0.17	0.51	0.34
EDD	0.50	0.29	0.63	0.11	0.39	0.44
SH	0.47	0.61	0.20	0.27	0.12	−0.07
LH	0.60	0.22	0.04	−0.13	0.16	−0.05
SH + LH	0.62	0.45	0.15	0.08	0.25	−0.07
MNT	0.14	0.38	0.35	0.16	0.47	0.34
			rms ratio			
Total	1.10	0.75	0.84	1.00	1.25	1.19
EDD	0.66	0.61	0.63	0.74	0.80	0.84
SH	0.48	0.26	0.18	0.46	0.50	0.18
LH	0.29	0.30	0.19	0.64	0.60	0.43
SH + LH	0.64	0.50	0.30	0.54	0.62	0.51
MNT	0.16	0.19	0.19	0.26	0.37	0.20

forcing increase from $m = 1$ to $m = 5$. Wavenumber 6, on the other hand, is simulated rather poorly.

The impact of mountains is significant only in $m = 2$ and results in an amplitude for the total simulation of this wavenumber which is close to the observed amplitude (Fig. 8, left column).

The transient eddies are also the main contributors to the anomalous wind fields in the tropics. The correlation for the $\hat{u}$ and $\hat{v}$ fields is much larger than for the low amplitude $\hat{T}$ field (Table 2). Since direct eddy forcing in the tropics is negligible, the large tropical response must be caused by wave propagation from the midlatitudes, which is possible because of the absence of tropical upper tropospheric easterlies in the model.

The large impact of the transient eddies on the strength and position of the GCM anomalies agrees very well with the results of KO. In that paper, the same was shown for observed seasonal mean anomalies in 400 mb winds.

c. *A closer look at the effects of transients*

The response to transient eddy forcing can further be divided into a part due to forcing in the momentum equations (mechanical transients) and a part resulting from forcing in the thermodynamic equation (thermal transients). The nature of the temperature responses, due to mechanical and thermal transient forcing alone, which are shown in Fig. 9a and 9b respectively, appears to be quite different. The response to thermal transients shows hardly any amplitude outside the high–low couplet at 60°N. It is therefore very similar to the response to sensible and latent heating. The pcc between 30° and 60°N is 0.53.

The response in $\hat{T}$ to mechanical transients exhibits much smaller scale features and has also considerable amplitude outside the midlatitudes. The correlation with the anomalies in the GCM experiment is much less. Both forcings give rise to a cold anomaly over the United States, while they seem to counteract each other over the northern part of Asia. The large values in $\hat{T}$, $\hat{u}$ and $\hat{v}$ over Canada in the experiment when all forcings are combined (Figs. 4, 5 and 6) appear to be almost entirely caused by the mechanical part of the transients.

The response to thermal transient forcing is strongly baroclinic whereas the response to the mechanical effects of transient eddies is essentially equivalent barotropic. Consequently, the mechanical forcing contributes substantially to the 400 mb wind response while its contribution to the response in $\hat{T}$ is somewhat smaller (Table 3). Also the remote tropical effects are mainly due to the mechanical part of the transient eddy forcing. In spite of the large amplitudes, due to this forcing, the pcc is low except for the response in $\hat{v}$. The response to thermal eddy forcing resembles the anomalies occurring in the GCM much better.

The baroclinic and barotropic nature of the responses to thermal and mechanical transient eddy forcing respectively was already noticed by Opsteegh and Vernekar (1982) in their simulation of the January standing wave pattern.

d. *Effects of tropical versus extratropical latent heating*

Finally, the separate effects of anomalous precipitation in and outside the tropics (0°–30°N) are examined. These effects, expressed in terms of pcc and rms ratio, are given in Table 4.

It is evident from Table 4 that these forcings counteract each other to a large extent. They give rise to correlations of opposite sign causing the rms ratio for the combined response to be smaller than the largest of the separate ones. This is true for the tropics as well as the extratropics.

The $\hat{T}$ response to latent heating in middle latitudes correlates well with the GCM anomalies in both midlatitudes and tropics. The rms ratio is close to 0.5 in both latitudinal belts, which means that midlatitudinal latent heating contributes significantly to the hemispheric temperature pattern.

The effect of tropical latent heat release in terms of the rms is large in the tropics but gives zero or negative correlations. The remote response to tropical latent heating is small. Branstator (1985a,b) also performed an analysis of a GCM SST anomaly experiment. He used a nondivergent barotropic vorticity-conserving model linearized around the control run's 300 mb wavy basic state. The forcing anomaly was introduced in his model by means of a vorticity source located directly over the tropical rainfall anomaly. The resulting midlatitude perturbation height pattern resembled the GCM pattern fairly well. So we cannot exclude the possibility that the remote effects of tropical latent heating will prove to be significant when the interaction with stationary eddies is included.

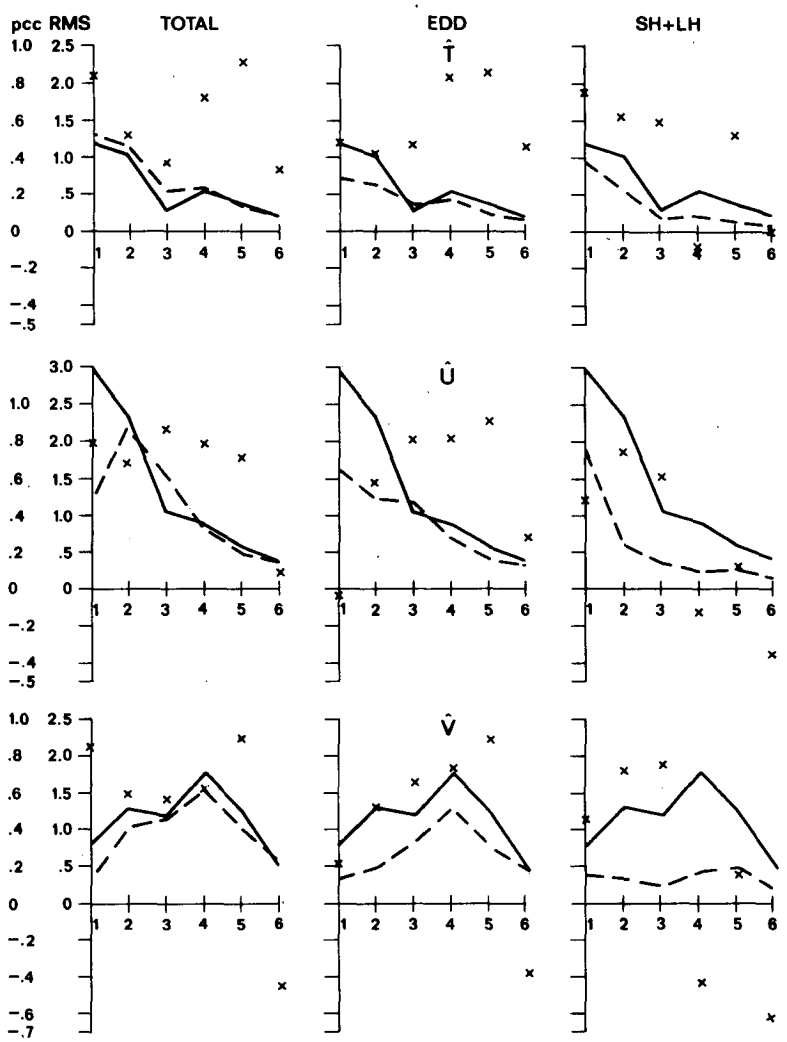

FIG. 8. Pattern correlation coefficient and root mean square of $\hat{T}$ at 600 mb, $\hat{u}$ and $\hat{v}$ at 400 mb for separate zonal wavenumbers and for a zone between 30° and 60°N. Pattern correlation coefficients are indicated by crosses. Dashed lines show the rms for the linear model's results, solid lines show the same quantity for the GCM experiment. The left column shows the results when the model is driven by all forcings combined. In the middle column the forcing is by transient eddies only and in the right column by diabatic heating only.

It appears that sensible heating and extratropical latent heating give rise to anomalous temperatures and zonal winds which are similar in pattern over the whole hemisphere (not shown). Thus, the extratropical precipitation seems to strengthen the impact of the sensible heat flux distribution at the surface.

5. Conclusions

With a linear steady state model, the importance of heating in the 40-day mean response of a GCM to a subtropical SST anomaly has been diagnosed. We have compared this effect with the (statistical) effect of transient eddies. We look upon the transient eddy terms in the time-averaged equations as fixed sources and sinks of momentum and heat. It appears that the transient eddies have a large impact on the strength of the anomalies. Because we analyzed a single GCM experiment, this conclusion cannot as yet be generalized. We also have to stress that we only considered a relatively short time period (40 days). On longer time scales, the relative importance of the eddies may be smaller although KO arrived at similar conclusions for observed seasonal mean anomalies. To what extent the anomalous eddy forcing is just a manifestation of the model's natural variability or that it is somehow related to the SST anomaly in the Atlantic cannot be answered within the context of our approach. As the anomalous

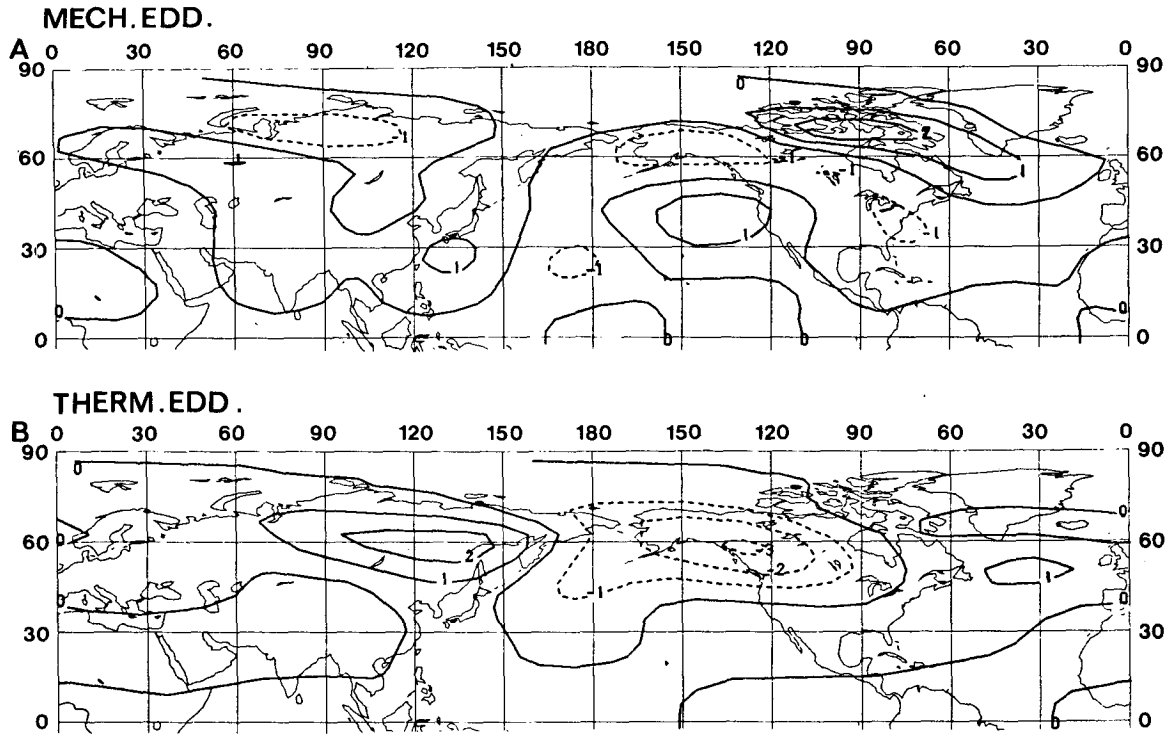

FIG. 9. Response of the linear model in $\hat{T}$ at 600 mb to mechanical (a) and thermal (b) transient eddy forcing. Units are in °K.

heat sources are not obviously connected to the SST anomaly, we speculate that the differences between both experiments reflect the model's natural variability. In KO it was suggested on the basis of a strong persistence in the anomalous transient eddy forcing during the 1982/83 El Niño event that the forcing was somehow linked to the SST anomaly in the tropical Pacific. In order to be able to provide a definite answer, we need to analyse a GCM SST anomaly experiment with an integration time sufficiently long to provide a stable climate for given boundary conditions. Obviously, in such an experiment all anomalous eddy forcing can be attributed to the differences in the boundary conditions.

The similarity between the time mean anomalies of the GCM experiment and the linear model's response is very high. The pattern correlation coefficients for $\hat{T}$ at 600 mb, $\hat{u}$ and $\hat{v}$ at 400 mb are 0.68, 0.63 and 0.61, respectively, for a strip between 30° and 60°N. The linear model's response to each of the three anomalous forcings (latent heating, sensible heating and transient eddy forcing) is positively correlated with the GCM anomaly pattern. The amplitudes of the response to anomalous transient eddy forcing is a factor of two to three larger than the simulated effects of anomalous sensible and latent heating.

The response to thermal transient forcing is strongly

TABLE 3. As in Table 1 but for mechanical and thermal transient eddy forcing.

	30°–60°N			0°–30°N		
Forcing	$\hat{T}$	$\hat{u}$	$\hat{v}$	$\hat{T}$	$\hat{u}$	$\hat{v}$
		pcc				
Mechanical EDD	0.20	−0.02	0.52	0.01	0.24	0.39
Thermal EDD	0.53	0.60	0.62	0.22	0.30	0.37
Total EDD	0.50	0.29	0.63	0.11	0.39	0.44
		rms ratio				
Mechanical EDD	0.36	0.56	0.50	0.63	0.74	0.75
Thermal EDD	0.49	0.32	0.23	0.35	0.45	0.22
Total EDD	0.66	0.61	0.63	0.74	0.80	0.84

TABLE 4. As in Table 1 but for tropical and extratropical latent heating.

	30°–60°N			0°–30°N		
Forcing	$\hat{T}$	$\hat{u}$	$\hat{v}$	$\hat{T}$	$\hat{u}$	$\hat{v}$
		pcc				
LH 0–30°N	−0.17	−0.40	−0.13	−0.32	0.03	−0.11
LH North of 30°N	0.51	0.57	0.13	0.45	0.12	0.15
Total LH	0.60	0.22	0.04	−0.13	0.16	−0.05
		rms ratio				
LH 0–30°N	0.26	0.30	0.20	1.02	0.94	0.50
LH North of 30°N	0.43	0.32	0.26	0.55	0.55	0.23
Total LH	0.29	0.30	0.19	0.64	0.60	0.43

baroclinic, whereas the response to the mechanical effects of transient eddies is essentially equivalent barotropic. Consequently, the mechanical forcing contributes substantially to the 400 mb wind response while its contribution to the response in $\hat{T}$ is smaller than the effect of thermal transient forcing.

The resulting effect of transient eddies is to increase the amplitude of the anomalies generated by anomalous heating. The thermal transient forcing enhances the temperature anomalies substantially, in spite of the fact that the initial tendencies that would be induced by this forcing act to destroy the observed temperature anomalies (compare Figs. 2 and 4). In our approach, we assume that the time-mean atmosphere is in equilibrium with the observed distribution of transient eddy forcing. In other words, the principal balance is between advection and eddy forcing. The anomalous time-mean circulation pattern needed to make this balance appears to be approximately in phase with the effects of anomalous sensible and latent heating. This may be purely coincidental. However, it is interesting to note that Held et al. (1986) argued that the mixing of heat and potential vorticity by transient eddies may destabilize the long waves resulting in an amplification rather than a reduction of the amplitude of these waves.

Acknowledgments. The assistance of P. R. Rowntree, A. Gilchrist and D. Mansfield of the British Meteorological Office in providing the GCM data is gratefully acknowledged. We are also grateful for the comments of the reviewers. We thank Birgit Kok for preparing the manuscript.

REFERENCES

Branstator, G., 1985a: Analysis of general circulation model sea-surface temperature anomaly simulations using a linear model. Part I: Forced solutions. *J. Atmos. Sci.*, **42**, 2225–2241.

——, 1985b: Analysis of general circulation model sea-surface temperature anomaly simulations using a linear model. Part II: Eigen-analysis. *J. Atmos. Sci.*, **42**, 2242–2254.

Held, I. M., R. T. Pierrehumbert and R. L. Panetta, 1986: Dissipative destabilization of external Rossby waves. *J. Atmos. Sci.*, **43**, 388–396.

Holopainen, E. O., 1984: Statistical local effect of synoptic-scale transient eddies on the time-mean flow in the northern extratropics in winter. *J. Atmos. Sci.*, **41**, 2505–2515.

Hoskins, B. J., and D. J. Karoly, 1981: The steady linear response of a spherical atmosphere to thermal and orographic forcing. *J. Atmos. Sci.*, **38**, 1179–1196.

Kok, C. J., and J. D. Opsteegh, 1985: On the possible causes of anomalies in seasonal mean circulation patterns during the 1982/83 El Niño event. *J. Atmos. Sci.*, **42**, 677–694.

Lau, N. C., 1979: The observed structure of tropospheric stationary waves and the local balances of vorticity and heat. *J. Atmos. Sci.*, **36**, 996–1016.

Opsteegh, J. D., and H. M. van den Dool, 1980: Seasonal differences in the stationary response of a linearized primitive equation model: Prospects for long-range weather forecasting? *J. Atmos. Sci.*, **37**, 2169–2185.

——, and A. D. Vernekar, 1982: A simulation of the January standing wave pattern including the effects of transient eddies. *J. Atmos. Sci.*, **39**, 734–744.

Rowntree, P. R., 1976: Response of the atmosphere to a tropical Atlantic ocean temperature anomaly. *Quart. J. Roy. Meteor. Soc.*, **102**, 607–625.

Simmons, A. J., 1982: The forcing of stationary wave motion by tropical heating. *Quart. J. Roy. Meteor. Soc.*, **108**, 503–534.

Youngblut, C., and T. Sasamori, 1980: The nonlinear effects of transient and stationary eddies on the winter mean circulation. Part 1: Diagnostic analysis. *J. Atmos. Sci.*, **37**, 1944–1957.